Highly sensitive and selective Love mode surface acoustic wave ammonia sensor based on graphene oxides operated at room-temperature

Q. B. Tang[a], Y. J. Guo[a,*], Y. L. Tang[b], G. D. Long[a], J. L. Wang[a], D. J. Li[c], X. T. Zu[c], J. Y. Ma[d], L. Wang[d], H. Torun[e], Y. Q. Fu[e,*]

[a] School of Physics, University of Electronic Science and Technology of China, Chengdu, 610054, P. R. China

[b] School of Physical Science and Technology, Southwest Jiaotong University, Chengdu, 610031, P. R. China

[c] Institute of Fundamental and Frontier Sciences, University of Electronic Science and Technology of China, Chengdu, 610054, P. R. China

[d] Sichuan Institute of Piezoelectric and Acousto-Optic Technology, Chongqing, 400060, P. R. China

[e] Faculty of Engineering and Environment, University of Northumbria, Newcastle upon Tyne, NE1 8ST, UK

Abstract: It is crucial to develop highly sensitive and selective sensors for ammonia, one of the most common toxic gases which have been widely used in pharmaceutical, chemical and manufacturing industries. In this study, graphene oxide (GO) film was spin-coated onto surfaces of ST-cut quartz surface acoustic wave (SAW) devices with a resonant frequency of 200 MHz for ammonia sensing. The oxygen-containing functional groups (such as hydroxyl and epoxy ones) on the surface of GO film strongly absorb ammonia molecules and thus increase the film stiffness. This is attributed to the main ammonia sensing mechanism of the Love mode SAW devices, which show not only a positive frequency shift of 620 Hz for 500 ppb ammonia gas, but also an excellent selectivity (as compared to other gases such as H_2, H_2S, CO and NO_2) and a good reproducibility, operated at room temperature of 22 ºC.

Keywords: Surface acoutic wave (SAW); graphene oxide (GO); ammonia sensor.

*Corresponding authors.

E-mail address:

Prof. Yuanjun Guo (guoyuanjun@uestc.edu.cn); Prof. Richard Yongqing Fu (richard.fu@northumbria.ac.uk)

1. Introduction

Ammonia, one of the most common toxic gases, is widely used in pharmaceutical, chemical and manufacturing industries. Ammonia is considered to be a very promising hydrogen carrier due to its high energy density, low cost, easy liquefaction which can be transported easily. In addition, ammonia is essential for carbon-free production of hydrogen [1, 2]. Due to its wide-range of applications, the risk for ammonia leakage or contamination in our daily life becomes quite high, and excessive inhalation of ammonia can lead to respiratory disease, severe headache, sore throat, loss of smell and chest pain. Occupational Safety and Health Administration, United States of Labor set a permissible exposure limit for ammonia at 50 ppm during a work day of eight hours. Therefore, it is critical to develop highly sensitive and highly selective ammonia sensors, and significant attention has recently been paid on detection and monitoring of ammonia along with other toxic gases [3-5].

Surface acoustic wave (SAW) technology has been well developed for gas sensing and particularly for ammonia sensing [6-13]. SAW devices generally have high sensitivity, fast response, good stability, and they offer ease of subsequent signal processing. The operation principle of a SAW gas sensor is based on the interaction of a sensitive film with the targeted gas molecules that results in changes in phase velocity and amplitude of the waves. Therefore, the concentration of the target gas can be measured by monitoring the changes in frequency or phase angle of the resonant frequency peaks [14]. Adding a sensitive layer material which has a strong affinity to

the targeted gas is an effective way to improve the sensitivity [15]. A variety of materials have been employed for the sensitive layers, including polymers [16-18], semiconducting metal oxides [7, 11, 19, 20], carbon nanomaterials [21, 22], and graphene and its derivatives [23, 24]. When these layers are deposited onto a quartz-based shear-horizontal SAW device, a Love mode SAW device can be developed, which has significantly improved the sensitivity due to the existence of the guiding layer for the SAWs [13].

Graphene derivatives (such as graphene oxide: GO, and reduced graphene oxide, rGO) have been reported to have larger surface areas and more chemically active sites than those of nanostructured metal oxides, conductive polymers, and carbon nanotubes [25]. In addition to their intrinsic advantages, their chemical and electrical properties are tunable based on their growth parameters. These characteristics are very attractive for gas sensing applications. GO, a precursor to graphene, contains a variety of oxygen-containing functional groups. It is generally accepted that these functional oxygen groups exist mainly in the form of hydroxyl groups and epoxy groups on the surface of the GO sheet, together with smaller amounts of carboxyl groups, carbonyl groups, quinone, lactones, and phenols at the edges of the GO sheet [26-28]. Due to the presence of these oxygen-containing groups, GO can be stably dispersed in many solvents, especially in water [29-31]. A uniform layer of GO can be obtained on various substrates by using simple methods such as dip coating, spray coating or spin coating [27]. In addition, GO possesses the 2D characteristics of graphene, which could

enhance the effective interactions with many analytes.

Various GO-based sensors have been reported for gas monitoring. GO-based SAW sensors have been demonstrated for the detections of humidity [24], NO_2 [32, 33], H_2 [34] and chemical warfare agents [35]. One of the advantages of using the GO for ammonia detection was demonstrated by Peng et al. [36] based on first-principles calculations, which revealed that the GO can be used to detect ammonia more efficiently than graphene. GO's surface-active defect sites such as epoxy and hydroxyl groups promote the interactions between ammonia molecules and GO. The GO has been widely used in optical [37] and impedance sensors [36] to detect ammonia. Generally, the impedance-based GO sensors are often needed to operate at elevated temperatures (e.g. often above 100°C) in order to increase their responses and recovery rates and sensitivities [38, 39]. However, when the operating temperature is higher than 200 °C, the oxygen-containing functional groups are decomposed, leading to an apparent degradation in sensitivity [40].

A good technique for the realization of precision sensing of ammonia operated at room temperature is SAW technology, especially those Love-mode SAW devices. Moreover, SAW sensors can be operated wirelessly with a low power consumption and a capability of remote operation. This is practically advantageous for toxic gas sensors. However, currently there are only a limited number of studies for the GO-based SAW sensors for the ammonia [41, 42], thus it is extremely valuable to prepare a SAW sensor based on the GO for ammonia sensing and study its sensing mechanisms.

In this work, we realized a GO-based Love mode SAW ammonia sensor on an ST cut quartz substrate, operated at a room temperature of 22 ºC. Its key sensing mechanism is mainly based on the increase of the sensing layer's stiffness when the ammonia molecules are adsorbed by the oxygen-containing functional group of GO, which are deposited onto the SAW surface. Our results indicate the presence of oxygen-containing functional groups also enhances sensitivity and selectivity of the sensor operated at room temperature.

2. Experimental methods

The two-port resonator SAW device was fabricated on an ST-cut quartz substrate using the conventional photolithography and metallization processes. Aluminum layer with a thickness of 200 nm was sputtered onto the ST-cut（42°75′） quartz substrate and then the interdigital transducers (IDT) were prepared using a lift-off process. The propagation direction of the generated SH-SAW is perpendicular to the crystallographic x-axis (90°-rotated). There are two sets of 30 pairs of IDTs on the SAW resonator. The period of IDT is 16 μm and the aperture is 3 mm. The center frequency of SAW devices was designed to be ~200 MHz, which is determined by the wave velocity on the piezoelectric substrate (3158 m/s) and the SAW wavelength (16 μm). The SAW devices had a center frequency of 200.02 MHz and an insertion loss of -8.82 dB, as shown in Figure 1. GO was produced using an improved Hummers' method [43]. The prepared GO was dissolved in deionized water, and then sonicated for one hour to prepare an aqueous solution with 2 mg/ml graphene oxide. The prepared GO solution was spin-

coated onto the SAW substrate at a spin-speed of 6000 rpm for 30 seconds, and then dried at 60 ºC for 10 minutes, and then the Love mode SAW device was obtained. The above processing cycle was repeated for five times to obtain a ~50 nm-thick GO sensing film. Our results showed that when the GO film thickness exceeds 50 nm, the current test setup does not work properly due to the limited gain of the amplifier circuit.

Field-emission scanning electron microscope (FE-SEM, FEI Inspect F50) was used to estimate the size of the prepared GO platelet and characterize the surface morphology of the prepared films. In addition, the GO film was characterized using various methods, including Raman spectroscopy (Alpha 300R with a laser beam wavelength of 488 nm), Fourier transform infrared spectroscopy (FTIR, Nicolet IS 10，in the range of 400–4000 cm^{-1}) and X-ray photoemission spectroscopy (XPS, Kratos Axis Ultra DLD, Al Kα radiation).

The resonant frequency of the SAW resonators was measured using a frequency counter (Agilent 53210A) with the help of a peripheral matching circuit. The SAW sensor was placed in a testing chamber with a volume of 20 L, which was pre-flowed with dry nitrogen gas before introducing ammonia. The standard purchased gas of ammonia (2% NH_3 with the balanced gas of N_2) was purchased from the National Institute of Testing Technology, China. The ammonia concentration in the testing chamber was precisely controlled using a dynamic volume method, e.g., 10 ml of standard ammonia gas was mixed with air (with a fixed ambient relative humidity, RH, of 40%) to obtain 10 ppm of ammonia gas in the gas chamber, and different ammonia

concentrations were obtained by controlling the volume of ammonia injected inside the chamber. During the gas sensing tests, the ambient temperature was controlled at 22°C and the ambient RH value was fixed at 40%. We monitored the resonant frequency and the electrical parameters of the Love-mode SAW device at different ammonia concentrations using a vector network analyzer (Hewlett Packard 8714C). In addition, the sheet resistance of the GO sensitive film and its changes after ammonia injection were measured using a source meter (Keithley 2400).

3. Results and discussions

3.1 Characterization of sensing film

An aqueous solution of 0.1 mg/ml of GO was coated on a silicon wafer and this GO layer was observed using the FE-SEM. The image is shown in Fig. 2, which shows that the prepared GO platelets have sizes ranging from 0.5 to 4 μm. Fig. 3 shows the SEM images of GO film, exhibiting a continuous membrane with some creases, and the inset image shows the cross-sectional SEM image, revealing that the thickness of the film is about 50 nm.

Fig. 4(a) shows the Raman spectrum of the GO film, with the D peak at 1356 cm^{-1} and G peak at 1581 cm^{-1}. The former corresponds to the structural defects caused by the hydroxyl and epoxy groups on the carbon surface [44], and the latter corresponds to the bond stretching of all carbon sp^2 components on the rings and chains [40, 45]. Other peaks at 120 cm^{-1}, 204 cm^{-1}, and 458 cm^{-1} are from the quartz substrate

[46]. FTIR spectra of the GO film is shown in Fig. 4(b), in which the oxygen-containing groups with different modes of vibrations can be detected, including epoxides (C-O-C, 1415 and ~918 cm^{-1}), carboxyl (COOH, 1599 cm^{-1}), basal hydroxy and hydroxy (edges Hydroxyl) (C-OH, 3100-3600 cm^{-1}). Both the Raman and FTIR results clearly showed that there are significant amount of epoxy, carboxyl, and hydroxy groups on the surface of the GO.

Fig. 5 shows XPS results of the GO film. Fig. 5(a) shows the XPS survey spectrum, from which the C/O atomic ratios of GO were measured to be 2.25. Figs. 5(b) and 5(c) are the C1s and O1s spectra of the GO film, respectively. The C1s spectrum consists of three well-resolved binding energy configurations at 284.9, 286.8, and 288.2 eV, corresponding to bonds of C-C, C-O and C=O, respectively. The C-C bonds reflect graphitized sp^2 hybridized carbon. The C-O bonds are attributed to the epoxy group and the hydroxyl group and phenol located on the surface of the GO. The C=O bonds are attributed to the carboxyl group and carbonyl group at the edge of the GO or at the defect. Figure 5(b) shows the O1s spectrum with the binding energy range of 528-536 eV, which can be deconvolved into C=O (531.6 eV), C-O-C (532.1 eV) and C-OH (533.7 eV). The C=O, C-O-C and C-OH bonds are corresponding to those of carbonyl/carboxy group, epoxy group and hydroxyl group on the GO, respectively. These results are consistent with those in the literature, indicating the presence of carbonyl/carboxy, epoxy and hydroxyl groups on surface of the GO [47].

3.2 Gas sensing performance and sensing mechanisms

Fig. 6(a) shows the dynamic responses of the Love mode sensor when it is exposed to ammonia concentrations between 0.5 ppm and 100 ppm at the room temperature of 22 °C and an RH of 40%. Our experimental data suggest that the resonant frequency increases with the concentration of the ammonia and the sensor can detect 500 ppb ammonia with an increase of the resonant frequency up to 620 Hz. It is also observed that the sensor's response increases with increasing the ammonia concentration. Fig. 6(b) shows that the frequency shift increases drastically at low concentrations of ammonia, whereas the reaction sites are gradually saturated at high concentrations due to the existence of limited functional groups that result in a modest frequency shift. If the frequency shift is re-drawn as a function of logarithm of ammonia concentration, a linear relationship can be obtained as shown in Fig. 6(c), which can be expressed using the following equation:

$$\Delta f = 1601 + 3904 \times \lg(C_{ppm}) \text{ (Hz)} \quad (1)$$

where Δf is the frequency shift in Hz and the C_{ppm} is the NH_3 concentration in ppm.

Fig. 6(d) shows the response and recovery times at different concentrations. Here, the response time is defined as the time required for the device's frequency shift to reach 90% of its final value. Similarly, the recovery time is defined as the time required for the device's frequency shift to return back to 10% of its total frequency shift value after the target gas is released. The recorded response times of the sensor exhibit some variations, but are all less than 250 s, whereas the recovery times are longer, with values

between 400 to 700 s. Table 1 summarizes the detection limits of various ammonia SAW sensors reported in the literature, and it is clear that the Love-mode SAW sensor we prepared shows the lowest detection limit.

Changes in the resonant frequency of the Love mode SAW devices during gas exposure can be attributed to various phenomena such as mass loading, acoustoelectric effect (electrical loading), and elastic loading [15].

The changes in the electrical properties (in particular, conductivity and dielectric constant) of a thin film is due to the adsorption and reaction of target gas molecules. Because the GO sensing layer has significant amount of epoxy, carboxyl, and hydroxy groups on its surface, and these will result in changes in the speed of sound, known as electroacoustic effect [15]. When the targeted gas molecules are introduced into the sensor surface, the frequency shift (Δf) will be positive if the conductivity of the sensing layer is decreased. Otherwise, the shift will be negative. The relationship between Δf and electroacoustic effect can be represented using the following equation [15]:

$$\frac{\Delta f}{f_0} = \frac{\Delta v}{v_0} \approx -\frac{k^2}{2}\left(\frac{\sigma_s^2}{\sigma_s^2 + v_0^2 c_s^2}\right) = -\frac{k^2}{2}\left(\frac{1}{1+\left(\frac{v_0 c_s}{\sigma_s}\right)^2}\right) \qquad (2)$$

where f_0 (~200 MHz) is the intrinsic resonant frequency; k^2 (0.11% for quartz) is the electromechanical coupling factor; v_0 (3158 m/s for quartz) is the unperturbed wave velocity for the SAW device; and c_s (0.5 pF cm^{-1}) is the sum of the dielectric permittivity of the substrate and the environment.

For the Love mode SAW sensor, the acoustoelectric effects depend on the changes of surface conductivity (σ_s) and resistance. Fig. 7(a) shows that the changes of the electrical conductivity of sensing layer will lead to frequency changes. As shown in Fig. 7(a), when the acoustoelectric parameters ($\xi = \sigma_s / v_0 c_s$, in which V_0 is 3158 m/s and C_s is 0.5 pF/cm) is between 0.01 and 100, an increase in the conductivity of the film causes a negative frequency shift, while a decrease in the conductivity of the film results in a positive frequency shift [15]. The sheet conductivity of GO film σ_s in the air is $5.4\times10^{-4} Sm^{-1}$, and the calculated acoustoelectric parameter is 340. The calculated values of the frequency shift due to the conductivity changes as shown in Fig. 7(a) are very small as compared to the experimental data which we obtained from this study. For example, assuming that the conductivity of the GO film is reduced to one percent of the previous one after injecting 10 ppm of ammonia gas, the calculated frequency shift caused by the acoustoelectric effect is only 9.6 Hz.

In order to further prove this conclusion experimentally, we measured the voltage vs. current results of the SAW electrode when the GO film was exposed to 500 ppm ammonia. We then calculated the resistance changes of the electrode, which are linked with the conductivity changes. The parameter for the resistance response of the SAW device was defined as $R = R_{air}/R_{gas}$, in which R_{air} is the resistance of GO film in ambient air and the R_{gas} is the resistance of GO film in ammonia and air mixed atmosphere. The calculated resistance response values of the SAW device are shown in Fig. 7(b) without any significant changes (i.e, varied from 1.0034 to 0.9985). Based on our theoretical

analysis and experimental data, we conclude that the electroacoustic effect is not dominant for the sensor's main frequency shift.

The mass loading on the film changes the resonant frequency of sensors as expressed in equation (3) [51]:

$$\frac{\Delta f}{f_0} = (k_1 + k_2) f_0^2 \rho_s \quad (3)$$

where $k_1 = -8.7 \times 10^{-8}$ m^{2}s kg^{-1} and $k_2 = -3.9 \times 10^{-9}$ m^{2}s kg^{-1} are material constants of the ST- cut quartz substrate; f_0 is the center frequency of the SAW that is not disturbed (~200 MHz); ρ_s is the surface density of the layer. When the mass density of the GO film is increased in ammonia gas, it will result in a negative frequency shift, and if its density is reduced, a positive frequency shift will occur.

When the GO is exposed to ammonia gas, the hydroxyl, carboxyl and epoxy groups on the sensitive film have a complex adsorption process with ammonia molecules with the help of water in the air [52-56]. The GO's adsorption of ammonia can be divided into physical adsorption and reactive adsorption. If reactive adsorption occurs (such as carboxyl and epoxy groups form amines after reacting with ammonia), the sensor will not be fully recovered and the repeatability will be poor [54,55]. Our experimental results show that the GO SAW ammonia sensor can be fully recovered, so we believe that the GO's adsorption of ammonia in this study is only a physical adsorption. When the GO layer physically adsorbs the ammonia gas molecules, the density of the sensitive layer will be increased and the resonance frequency shift will be decreased, thus resulting in a negative frequency shift. However, we have

systematically observed an increase in resonant frequency with the increase of gas concentration. Therefore, we believe the mass loading is not the key sensing mechanism for our sensor.

Another major influence for the frequency shift of the SAW device is the elastic loading [57]. When the sensing membrane adsorbs molecules, its viscoelasticity changes, and the generated stress or strain can partially be transmitted to the substrate. If there is a densification effect, the resonant frequency will increase. The elastic loading could be the dominant mechanism for the increase in the resonant frequency that we observed in this study. The frequency change due to the elastic loading can be expressed using the following equation[58]:

$$\frac{\Delta f}{f_0} = c_e f_0 h\left(\left(\frac{4u}{v_0^2}\right)\times\left(\frac{u+\lambda}{u+2\lambda}\right)\right) \tag{4}$$

where c_e is the sensitivity coefficients of elasticity, f_0 is the unperturbed frequency, h is film thickness, v_0 is the unperturbed SAW velocity, λ is the bulk modulus of elasticity, and u is the shear modules of elasticity. When the value of u is small ($\approx 10^6 Pa$), elastic loading can be negligible. For a large value of shear modulus ($\approx 10^9 Pa$), the elastic loading becomes critical and can induce a positive frequency shift [59].

According to previous reports [60], λ and u can be expressed by Young's modulus and Poisson's ratio as follows:

$$u = \frac{E}{2(1+v)} \tag{5}$$

and

$$\lambda = \frac{E}{2(1+v)} \tag{6}$$

where E and v are the Young's modulus and Poisson's ratio of the materials, respectively. Therefore, we can rewrite Eq. (3) as follows [57]:

$$\frac{\Delta f}{f_0} = c_e f_0 h\left(\left(\frac{4u}{v_0^2}\right)E \times \left(\frac{4v-5}{5v^2+v-4}\right)\right) \tag{7}$$

GO has a large Young's modulus, tens of GPa [61,62]. FTIR and XPS results in Section 3.1 show that different hydroxyl, carboxyl and epoxy groups exist on the surface of GO film. The hydroxyl groups and epoxy groups on GO film have shown large adsorption energies for ammonia molecules [36], indicating that GO has good adsorption to ammonia. Due to the network structure of GO and the small size of ammonia molecules, the ammonia molecules could easily be filled within the gaps between different GO atomic layers, thus increasing the stiffness of film, and resulting in a positive frequency shift, which is the same with the experimental result.

We further tested the selectivity of our GO SAW sensor against various major gas targets. Fig. 9(a) shows the sensor's dynamic responses to different gases. The concentrations of H_2, H_2S, CO and NO_2 are 50 ppm each, whereas that of NH_3 is 20 ppm. The GO SAW sensor is insensitive to H_2 and CO gases. It also shows minor responsivity to NO_2 and H_2S gases with the measured frequency shift values being less than 600 Hz. Whereas this GO SAW sensor shows a significant response to ammonia gas with measured frequency shift values of as large as 6700 Hz. Results showed that

our GO SAW sensor has an excellent selectivity for NH_3 gas.

Peng et al. reported that the oxygen-containing functional groups of GO (such as hydroxyl groups and epoxy groups) have good adsorption capability to ammonia [36]. Ammonia is highly soluble in water (volume ratio of ammonia and water is 1:700), so the surface of GO can effectively absorb both moisture and ammonia. In addition, ammonia incorporated by GO forms a new adsorption center to enhance the adsorption of ammonia [53]. Ammonia adsorption by the GO layers increases the stiffness of the sensitive layer, resulting in a large positive shift, thus explaining its excellent selectivity.

Finally, we tested the repeatability of our Love mode SAW sensor to the ammonia gas. Fig. 9(b) shows the measured dynamic responses of our sensor to 20 ppm NH_3 exposure for four successive cycles. The measured frequency shifts are 6.86 kHz, 7.01 kHz, 7.09 kHz, 7.33 kHz, respectively, after each of the four cycles. The variation in the resonant frequency is less than 5%, indicating the good repeatability of the SAW sensor.

4. Conclusions

We have developed the Love mode SAW resonators coated with GO sensing film on ST-cut quartz substrates for the detection of ammonia at room temperature of 22 ^{o}C. The sensor exhibits good responses to NH_3 gas, and it can detect 500 ppb NH_3 gas exposure with a positive frequency shift of 620 Hz. In addition, we characterized the relevant sensing parameters of our device. We measured response times less than 250 s and recovery times less than 700 s at room temperature. We also observed excellent

selectivity against major gas targets of H_2, H_2S, CO, NO_2 and good reproducibility at room temperature. In addition to demonstration of the sensing performance, we have systematically investigated the dominant sensing mechanism of our sensor by evaluating mass loading effect, acoustoelectric effect, and elastic loading effect. For this purpose, we characterized the structure of the sensor using XPS, Raman, and FTIR analyses. Results confirm the presence of different hydroxyl groups, carboxyl groups, and epoxy on the GO film. When exposed to ammonia, these oxygen-containing functional groups adsorb ammonia molecules, and increase the stiffness of the film, which is identified as the main reason for the positive frequency shift of the sensor.

Acknowledgments

The authors acknowledge the support by the Fundamental Research Funds for the Central Universities (A03018023801119), Funding supports from UK Engineering Physics and Science Research Council (EPSRC EP/P018998/1), Newton Mobility Grant (IE161019) through Royal Society and NFSC, and Royal academy of Engineering UK-Research Exchange with China and India are also acknowledged.

References

[1] R Lan, JT Irvine, S Tao (2012) Ammonia and related chemicals as potential indirect hydrogen storage materials, International Journal of Hydrogen Energy 37: 1482-1494.

[2] K Nagaoka, T Eboshi, Y Takeishi, et al. (2017) Carbon-free H_2 production from ammonia triggered at room temperature with an acidic RuO_2/γ-Al_2O_3 catalyst, Science advances 3: e1602747.

[3] B Timmer, W Olthuis, A Van Den Berg (2005) Ammonia sensors and their applications—a review, Sensors and Actuators B: Chemical 107: 666-677.

[4] N Joshi, V Saxena, A Singh, et al. (2014) Flexible H2S sensor based on gold modified polycarbazole films, Sensors and Actuators B: Chemical 200: 227-234.

[5] J Zhang, Z Qin, D Zeng, C Xie (2017) Metal-oxide-semiconductor based gas sensors: screening, preparation, and integration, Phys. Chem. Chem. Phys. 19: 6313-6329.

[6] L Bo, C Xiao, C Hualin, et al. (2016) Surface acoustic wave devices for sensor applications, Journal of Semiconductors 37: 021001.

[7] Y Tang, D Ao, W Li, X Zu, S Li, YQ Fu (2018) NH_3 sensing property and mechanisms of quartz surface acoustic wave sensors deposited with SiO_2, TiO_2, and SiO_2-TiO_2 composite films, Sensors and Actuators B: Chemical 254: 1165-1173.

[8] Y Tang, Z Li, J Ma, et al. (2015) Highly sensitive surface acoustic wave (SAW) humidity sensors based on sol–gel SiO_2 films: Investigations on the sensing property and mechanism, Sensors and Actuators B: Chemical 215: 283-291.

[9] Y-L Tang, Z-J Li, J-Y Ma, Y-J Guo, Y-Q Fu, X-T Zu (2014) Ammonia gas sensors based on ZnO/SiO_2 bi-layer nanofilms on ST-cut quartz surface acoustic wave devices, Sensors and Actuators B: Chemical 201: 114-121.

[10]Y-L Tang, Z-J Li, J-Y Ma, et al. (2014) Highly sensitive room-temperature surface acoustic wave (SAW) ammonia sensors based on Co_3O_4/SiO_2 composite films, J. Hazard. Mater. 280: 127-133.

[11]S-Y Wang, J-Y Ma, Z-J Li, et al. (2015) Surface acoustic wave ammonia sensor based on ZnO/SiO_2 composite film, Journal of hazardous materials 285: 368-374.

[12]W Li, Y Guo, Y Tang, et al. (2017) Room-temperature ammonia sensor based on ZnO nanorods deposited on ST-cut quartz surface acoustic wave devices, Sensors 17: 1142.

[13]YQ Fu, J Luo, N-T Nguyen, et al. (2017) Advances in piezoelectric thin films for acoustic biosensors, acoustofluidics and lab-on-chip applications, Progress in Materials Science 89: 31-91.

[14]J Devkota, PR Ohodnicki, DW Greve (2017) SAW Sensors for Chemical Vapors and Gases, Sensors (Basel) 17.

[15]WP Jakubik (2011) Surface acoustic wave-based gas sensors, Thin Solid Films 520: 986-993.

[16]JW Grate, M Klusty, RA McGill, MH Abraham, G Whiting, J Andonian-Haftvan (1992) The predominant role of swelling-induced modulus changes of the sorbent phase in determining the responses of polymer-coated surface acoustic wave vapor sensors, Anal. Chem. 64: 610-624.

[17]SJ Martin, GC Frye, SD Senturia (1994) Dynamics and response of polymer-

coated surface acoustic wave devices: effect of viscoelastic properties and film resonance, Anal. Chem. 66: 2201-2219.

[18]A Tretjakov, V Syritski, J Reut, R Boroznjak, A Öpik (2016) Molecularly imprinted polymer film interfaced with surface acoustic wave technology as a sensing platform for label-free protein detection, Anal. Chim. Acta 902: 182-188.

[19]W Luo, Q Fu, D Zhou, J Deng, H Liu, G Yan (2013) A surface acoustic wave H2S gas sensor employing nanocrystalline SnO2 thin film, Sensors and Actuators B: Chemical 176: 746-752.

[20] Z Li, H Li, Z Wu, et al. (2019) Advances in designs and mechanisms of semiconducting metal oxide nanostructures for high-precision gas sensors operated at room temperature, Materials Horizons 6: 470-506.

[21]M Penza, F Antolini, MV Antisari (2004) Carbon nanotubes as SAW chemical sensors materials, Sensors and Actuators B: Chemical 100: 47-59.

[22]M Penza, F Antolini, M Vittori-Antisari (2005) Carbon nanotubes-based surface acoustic waves oscillating sensor for vapour detection, Thin Solid Films 472: 246-252.

[23]R Arsat, M Breedon, M Shafiei, et al. (2009) Graphene-like nano-sheets for surface acoustic wave gas sensor applications, Chem. Phys. Lett. 467: 344-347.

[24]W Xuan, M He, N Meng, et al. (2014) Fast response and high sensitivity ZnO/glass surface acoustic wave humidity sensors using graphene oxide sensing layer, Sci. Rep. 4: 7206.

[25]SS Varghese, S Lonkar, KK Singh, S Swaminathan, A Abdala (2015) Recent advances in graphene based gas sensors, Sensors and Actuators B: Chemical 218: 160-183.

[26]Y Zhu, S Murali, W Cai, et al. (2010) Graphene and graphene oxide: synthesis, properties, and applications, Adv. Mater. 22: 3906-3924.

[27]X Li, G Zhang, X Bai, et al. (2008) Highly conducting graphene sheets and Langmuir–Blodgett films, Nature nanotechnology 3: 538.

[28]G Eda, M Chhowalla (2010) Chemically derived graphene oxide: towards large‐area thin‐film electronics and optoelectronics, Adv. Mater. 22: 2392-2415.

[29]R Bissessur, SF Scully (2007) Intercalation of solid polymer electrolytes into graphite oxide, Solid State Ionics 178: 877-882.

[30]D Chen, H Feng, J Li (2012) Graphene oxide: preparation, functionalization, and electrochemical applications, Chem. Rev. 112: 6027-6053.

[31]J Paredes, S Villar-Rodil, A Martínez-Alonso, J Tascon (2008) Graphene oxide dispersions in organic solvents, Langmuir 24: 10560-10564.

[32]MG Chung, DH Kim, HM Lee, et al. (2012) Highly sensitive NO2 gas sensor based on ozone treated graphene, Sensors and Actuators B: Chemical 166: 172-176.

[33]T Pustelny, S Drewniak, M Setkiewicz, et al. (2013) The sensitivity of sensor structures with oxide graphene exposed to selected gaseous atmospheres, Bulletin of the Polish Academy of Sciences: Technical Sciences 61: 705-710.

[34]M Proceka, Z Opilskia, J Jagiellob, L Lipinskab (2013) Investigations of SAW

Structures with oxide graphene layer to detection of selected gases.

[35]I Sayago, D Matatagui, MJ Fernández, et al. (2016) Graphene oxide as sensitive layer in Love-wave surface acoustic wave sensors for the detection of chemical warfare agent simulants, Talanta 148: 393-400.

[36]Y Peng, J Li (2013) Ammonia adsorption on graphene and graphene oxide: a first-principles study, Frontiers of Environmental Science & Engineering 7: 403-411.

[37]L Sansone, V Malachovska, P La Manna, et al. (2014) Nanochemical fabrication of a graphene oxide-based nanohybrid for label-free optical sensing with fiber optics, Sensors and Actuators B: Chemical 202: 523-526.

[38]S Basu, P Bhattacharyya (2012) Recent developments on graphene and graphene oxide based solid state gas sensors, Sensors and Actuators B: Chemical 173: 1-21.

[39]SS Varghese, S Lonkar, K Singh, S Swaminathan, A Abdala (2015) Recent advances in graphene based gas sensors, Sensors and Actuators B: Chemical 218: 160-183.

[40]S Prezioso, F Perrozzi, L Giancaterini, et al. (2013) Graphene oxide as a practical solution to high sensitivity gas sensing, The Journal of Physical Chemistry C 117: 10683-10690.

[41]A Afzal, N Iqbal, A Mujahid, R Schirhagl (2013) Advanced vapor recognition materials for selective and fast responsive surface acoustic wave sensors: a review, Anal. Chim. Acta 787: 36-49.

[42]Z Xu, YJ Yuan (2018) Implementation of guiding layers of surface acoustic wave devices: A review, Biosens. Bioelectron. 99: 500-512.

[43]J Chen, B Yao, C Li, G Shi (2013) An improved Hummers method for eco-friendly synthesis of graphene oxide, Carbon 64: 225-229.

[44]D Yang, A Velamakanni, G Bozoklu, et al. (2009) Chemical analysis of graphene oxide films after heat and chemical treatments by X-ray photoelectron and Micro-Raman spectroscopy, Carbon 47: 145-152.

[45]J Wang, B Singh, J-H Park, et al. (2014) Dielectrophoresis of graphene oxide nanostructures for hydrogen gas sensor at room temperature, Sensors and Actuators B: Chemical 194: 296-302.

[46]L Ding, W Zhou, TP McNicholas, et al. (2009) Direct observation of the strong interaction between carbon nanotubes and quartz substrate, Nano Research 2: 903.

[47]M Cittadini, M Bersani, F Perrozzi, L Ottaviano, W Wlodarski, A Martucci (2014) Graphene oxide coupled with gold nanoparticles for localized surface plasmon resonance based gas sensor, Carbon 69: 452-459.

[48]T Lin, Y Li, H Hao, I Fang, C Yang, D Yao (2011) Surface acoustic wave gas sensor for monitoring low concentration ammonia 2011 16th International Solid-State Sensors, Actuators and Microsystems ConferenceIEEE.

[49]Y Pan, N Mu, B Liu, B Cao, W Wang, L Yang (2018) A Novel Surface Acoustic Wave Sensor Array Based on Wireless Communication Network, Sensors 18: 2977.

[50]C-Y Shen, S-Y Liou (2008) Surface acoustic wave gas monitor for ppm ammonia detection, Sensors and Actuators B: Chemical 131: 673-679.

[51]H Wohltjen (1984) Mechanism of operation and design considerations for surface acoustic wave device vapour sensors, Sensors and Actuators 5: 307-325.

[52]C Petit, M Seredych, TJ Bandosz (2009) Revisiting the chemistry of graphite oxides and its effect on ammonia adsorption, Journal of Materials Chemistry 19: 9176-9185.

[53]M Seredych, TJ Bandosz (2009) Combined role of water and surface chemistry in reactive adsorption of ammonia on graphite oxides, Langmuir 26: 5491-5498.

[54] Zhu S, Sun H, Liu X, et al (2017). Room-temperature NH_3 sensing of graphene oxide film and its enhanced response on the laser-textured silicon[J]. Scientific reports, 7(1): 14773.

[55] Bannov A, Prášek J, Jašek O, et al (2017). Investigation of pristine graphite oxide as room-temperature chemiresistive ammonia gas sensing material[J]. Sensors, ,17(2): 320.

[56]M Seredych, AV Tamashausky, TJ Bandosz (2010) Graphite oxides obtained from porous graphite: the role of surface chemistry and texture in ammonia retention at ambient conditions, Advanced Functional Materials 20: 1670-1679.

[57]VB Raj, H Singh, AT Nimal, MU Sharma, M Tomar, V Gupta (2017) Distinct detection of liquor ammonia by ZnO/SAW sensor: Study of complete sensing mechanism, Sensors and Actuators B: Chemical 238: 83-90.

[58]V Bhasker Raj, AT Nimal, Y Parmar, MU Sharma, V Gupta (2012) Investigations on the origin of mass and elastic loading in the time varying distinct response of ZnO SAW ammonia sensor, Sensors and Actuators B: Chemical 166-167: 576-585.

[59]M Thompson, DC Stone (1997) Surface-launched acoustic wave sensors: chemical sensing and thin-film characterization. Wiley-Interscience,

[60]SL Hietala, VM Hietala, CJ Brinker (2001) Dual SAW sensor technique for determining mass and modulus changes, IEEE transactions on ultrasonics, ferroelectrics, and frequency control 48: 262-267.

[61]JW Suk, RD Piner, J An, RS Ruoff (2010) Mechanical properties of monolayer graphene oxide, ACS nano 4: 6557-6564.

[62]DA Dikin, S Stankovich, EJ Zimney, et al. (2007) Preparation and characterization of graphene oxide paper, Nature 448: 457.

FIGURE CAPTIONS

Figure 1. Transmission signal S_{21} of the ST-cut quart SAW resonators.

Figure 2. Optical microscope image showing the feature of GO platelet (marked with a circle)

Figure 3.Top-view and cross-view SEM images of GO film.

Figure 4. (a) Raman spectra of GO film showing the existence of D peak and G peak;(b) FTIR spectra of GO film showing the existence of epoxides, carboxyl, hydroxyl and phenolic groups.

Figure 5. XPS spectra of GO film. (a) high resolution XPS spectrum of C 1s; (b) high resolution XPS spectrum of O 1s.

Figure 6. (a) Dynamic frequency responses of the GO SAW sensor exposed to different concentrations of NH_3 gas; (b) frequency shift of the sensor exposed to different NH_3 concentrations; (c) frequency shift with a log function of ammonia concentration; (d) response and recovery times of the sensor at different NH_3 concentrations.

Figure 7. (a) Relationship between normalized frequency shifts with different acoustoelectric parameters when exposed to the ammonia gases with different concentrations; (b) Electrical resistance responses ($R=R_{air}/R_{gas}$) of the GO film when exposed to 500 ppm NH_3.

Figure 8. The reaction relationship between GO oxygen-containing functional groups and ammonia after adsorption of NH_3.

Figure 9. (a) Dynamic responses of the SAW sensor when exposed to different types of gases; (b) Dynamic responses of the sensor to NH_3 gas of 20 ppm for successive four cycles.

Fig.1

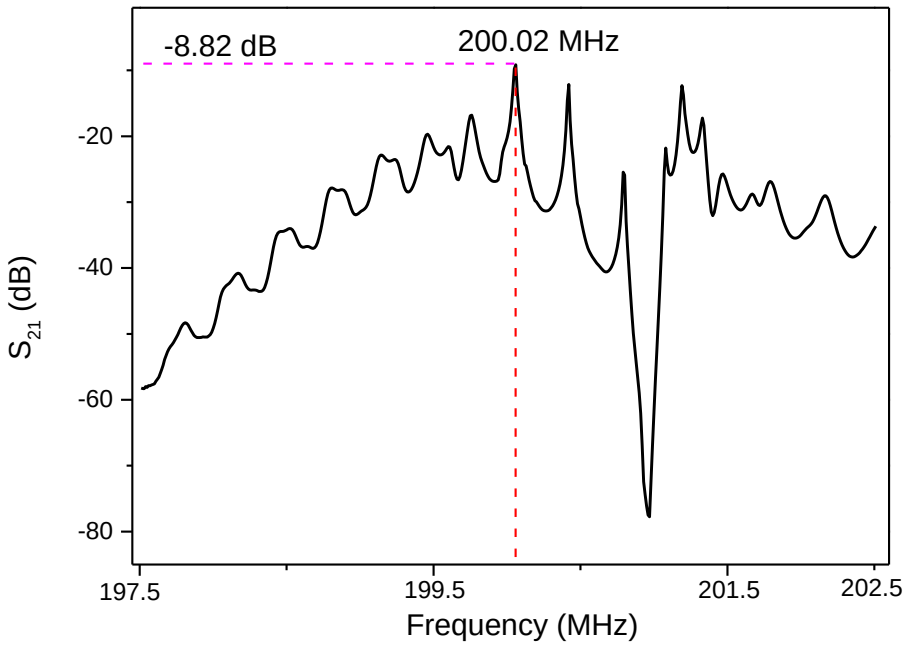

Fig.2

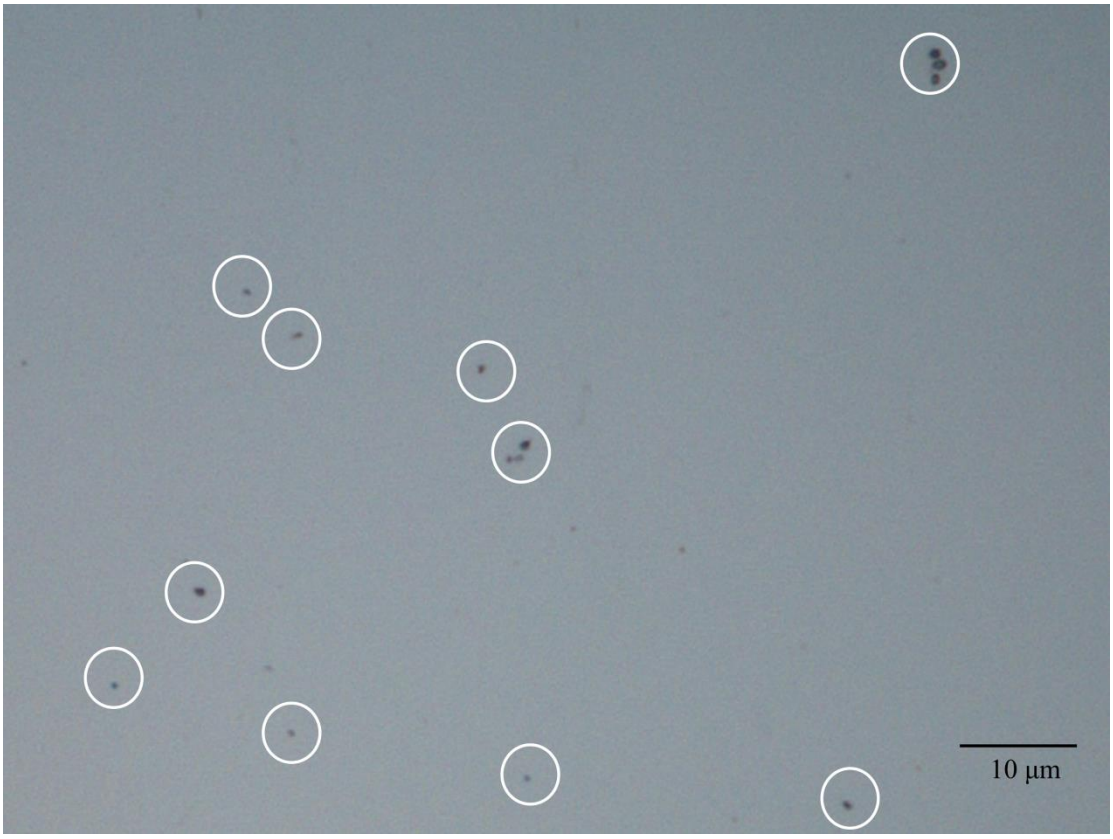
10 µm

Fig.3

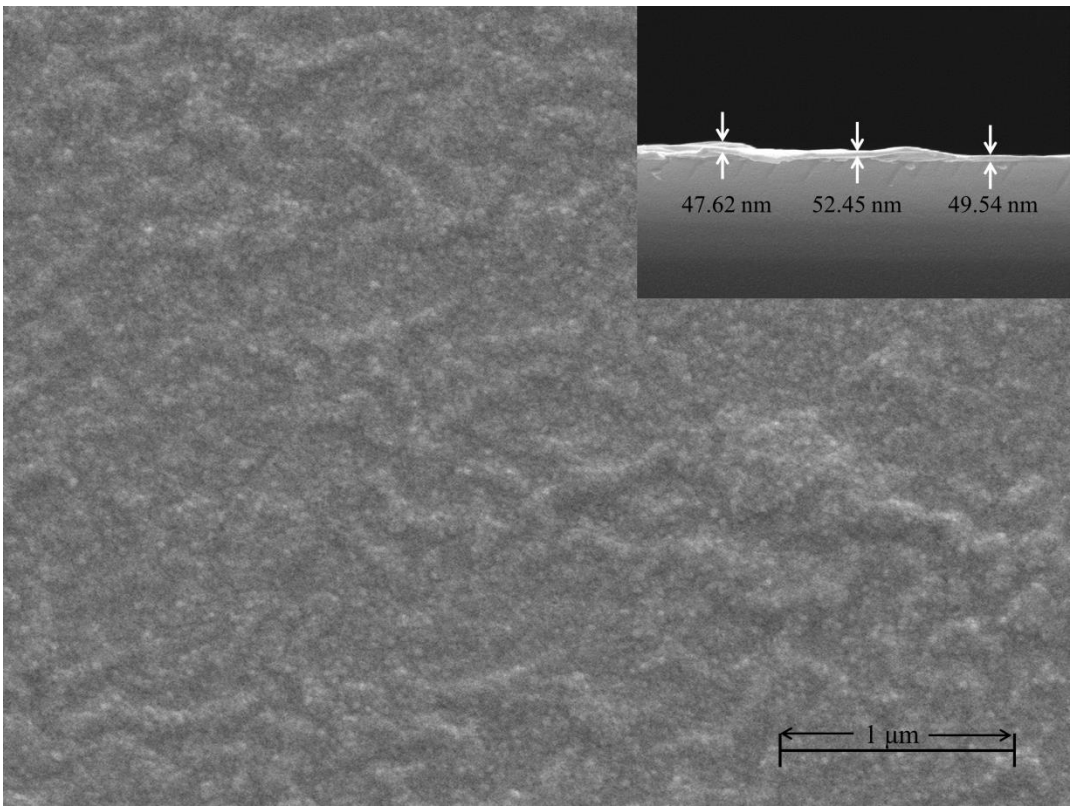
47.62 nm
52.45 nm
49.54 nm
1 µm

Fig.4(a)

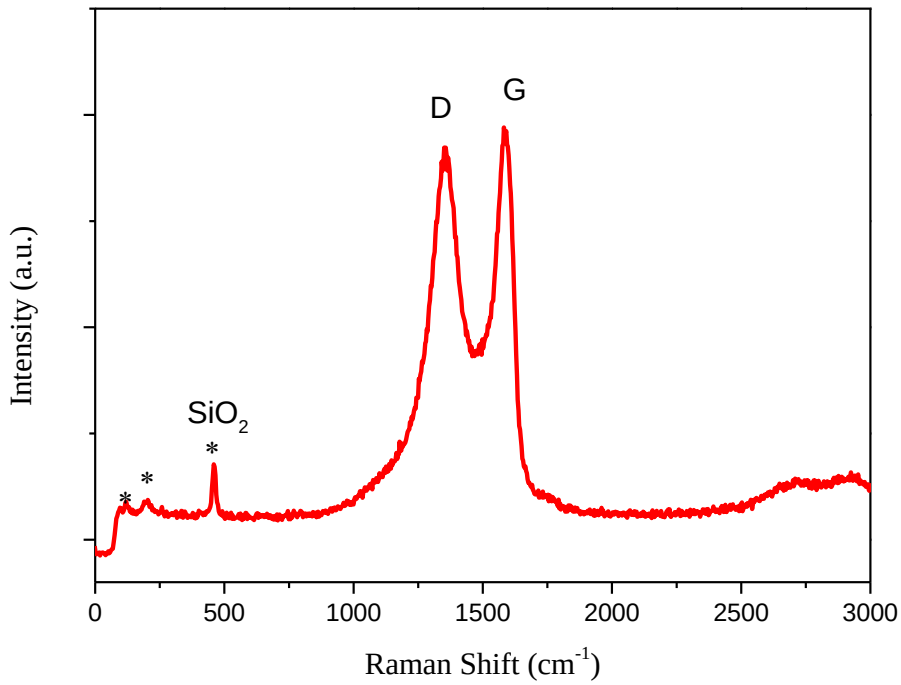
D
G
SiO2
*
*
*
Intensity (a.u.)
0
500
1000
1500
2000
2500
3000
Raman Shift (cm-1)

Fig.4(b)

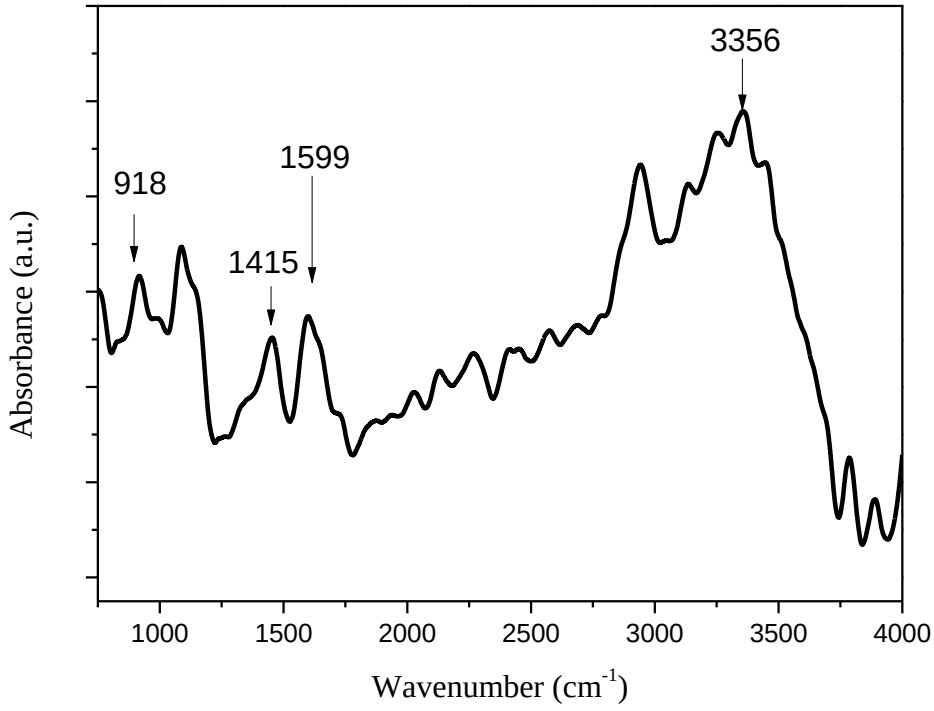
3356
1599
918
1415
Absorbance (a.u.)
1000
1500
2000
2500
3000
3500
4000
Wavenumber (cm-1)

Fig.5(a)

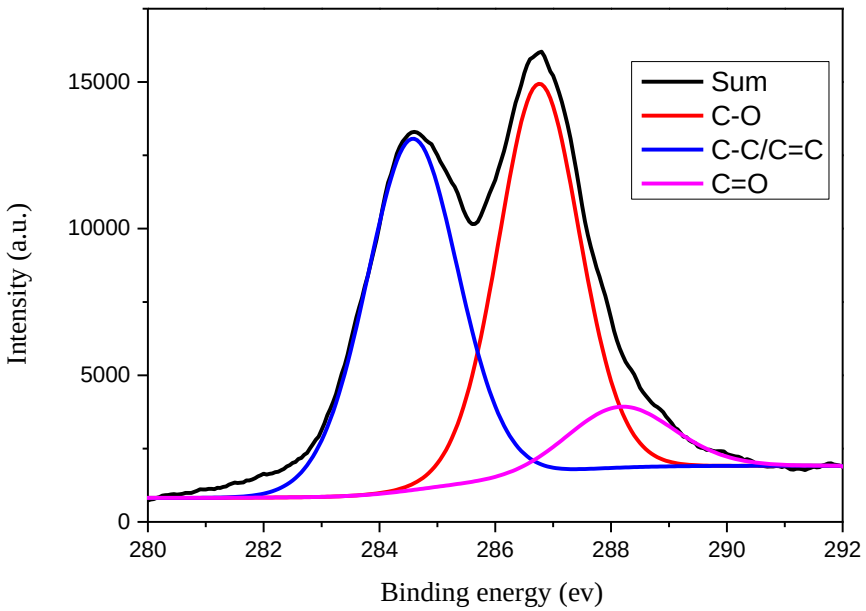
Sum
C-O
C-C/C=C
C=O
15000
10000
5000
0
Intensity (a.u.)
280
282
284
286
288
290
292
Binding energy (ev)

Fig.5(b)

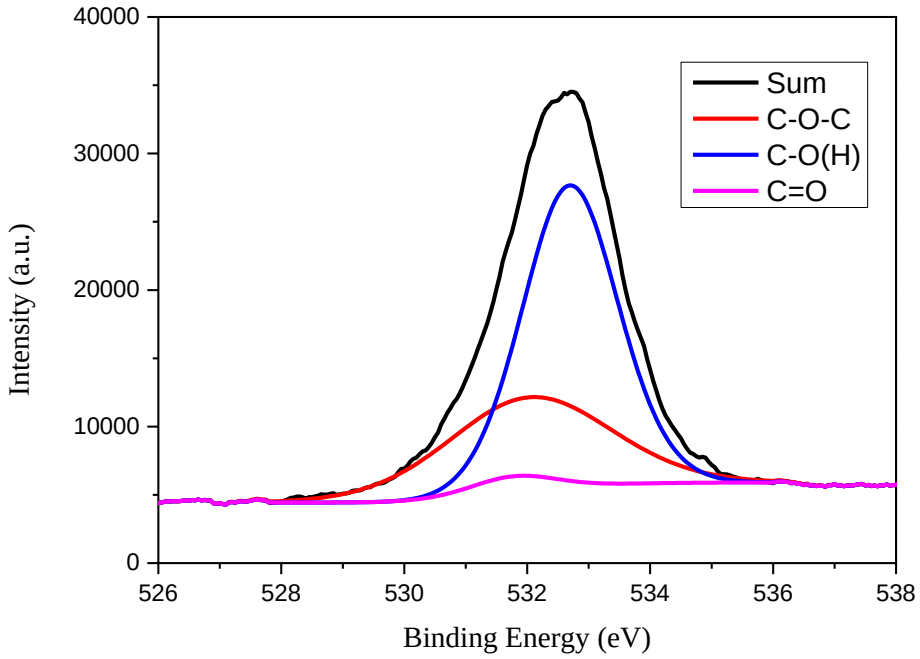
40000
30000
20000
10000
0
Intensity (a.u.)
526
528
530
532
534
536
538
Binding Energy (eV)
Sum
C-O-C
C-O(H)
C=O

Fig.6(a)

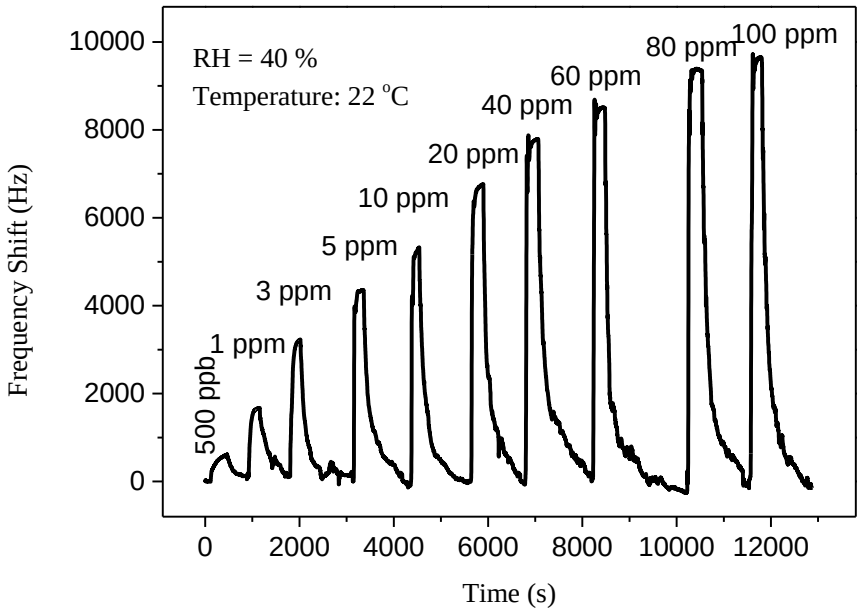
RH = 40 %
Temperature: 22 °C
500 ppb
1 ppm
3 ppm
5 ppm
10 ppm
20 ppm
40 ppm
60 ppm
80 ppm
100 ppm
Frequency Shift (Hz)
Time (s)
0
2000
4000
6000
8000
10000
12000

Fig.6(b)

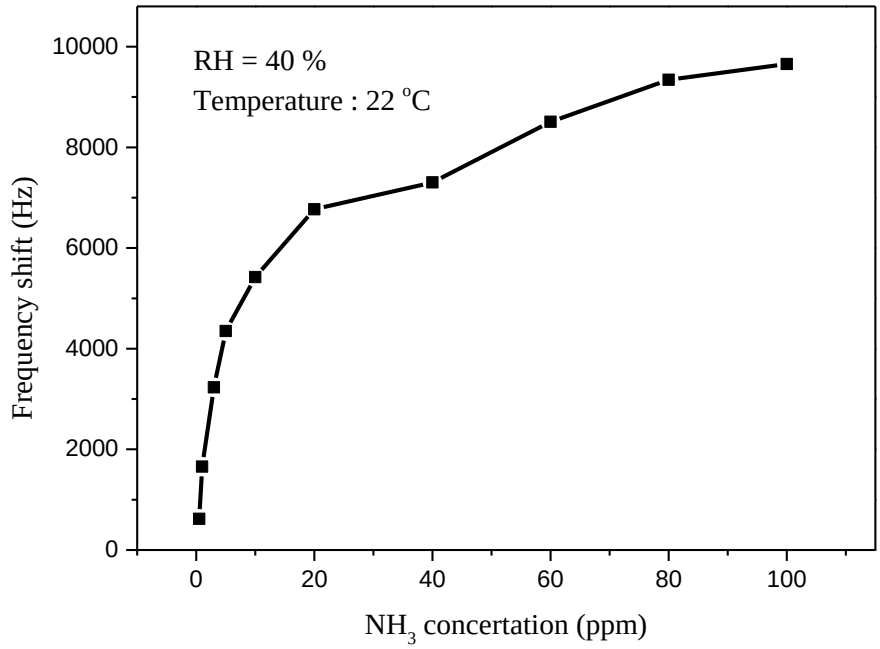
RH = 40 %
Temperature : 22 °C
Frequency shift (Hz)
NH3 concertation (ppm)
0
2000
4000
6000
8000
10000
0
20
40
60
80
100

Fig.6(c)

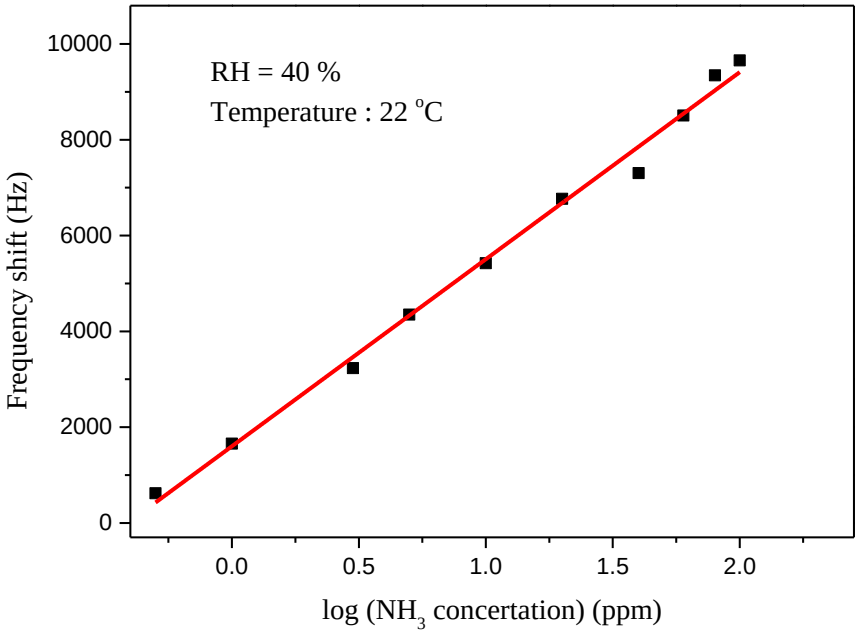
RH = 40 %
Temperature : 22 °C
Frequency shift (Hz)
log (NH3 concertation) (ppm)
10000
8000
6000
4000
2000
0
0.0
0.5
1.0
1.5
2.0

Fig.6(d)

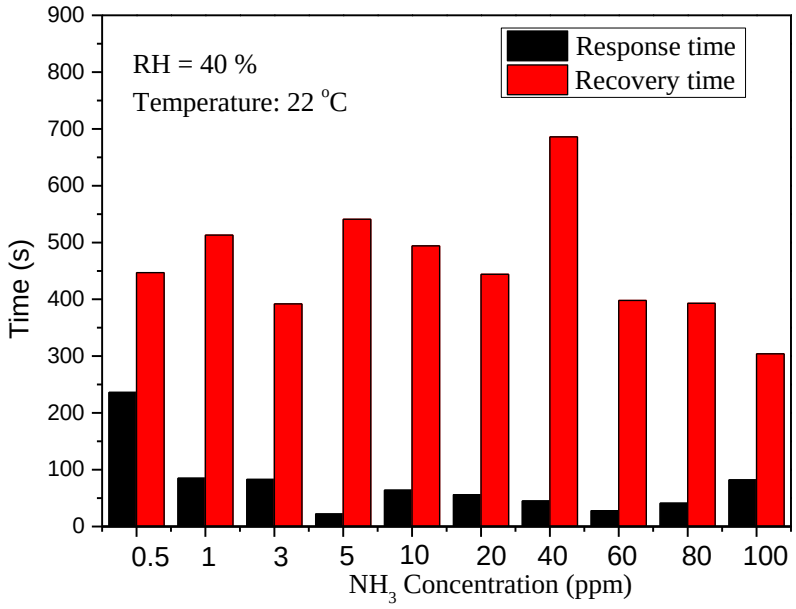
RH = 40 %
Temperature: 22 °C
Response time
Recovery time
Time (s)
900
800
700
600
500
400
300
200
100
0
0.5
1
3
5
10
20
40
60
80
100
NH3 Concentration (ppm)

Fig.7(a)

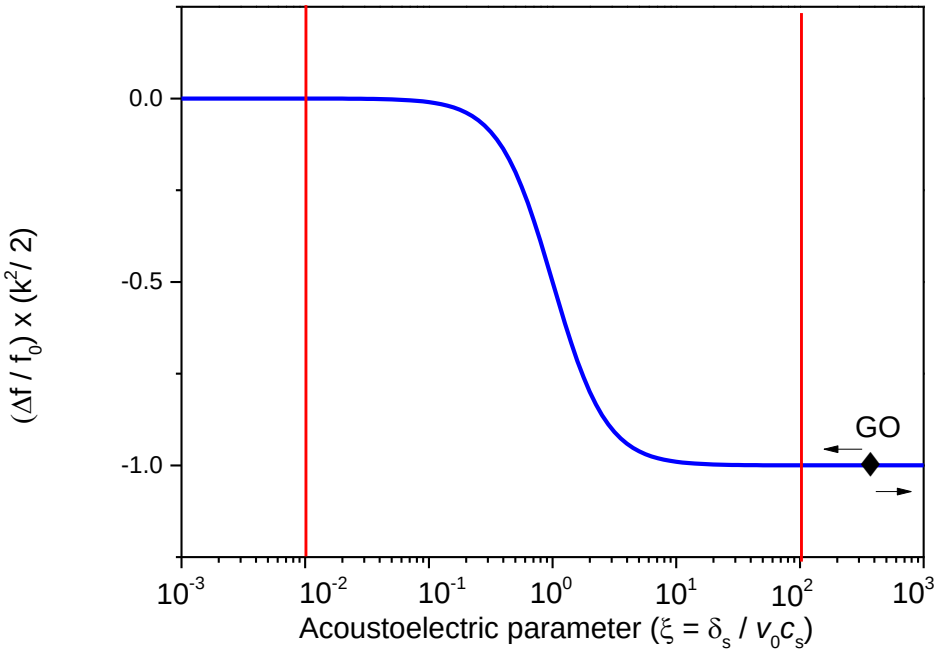
0.0
-0.5
-1.0
GO
10^{-3}
10^{-2}
10^{-1}
10^{0}
10^{1}
10^{2}
10^{3}
$(\Delta f / f_0) \times (k^2/2)$
Acoustoelectric parameter ($\xi = \delta_s / v_0 c_s$)

Fig.7(b)

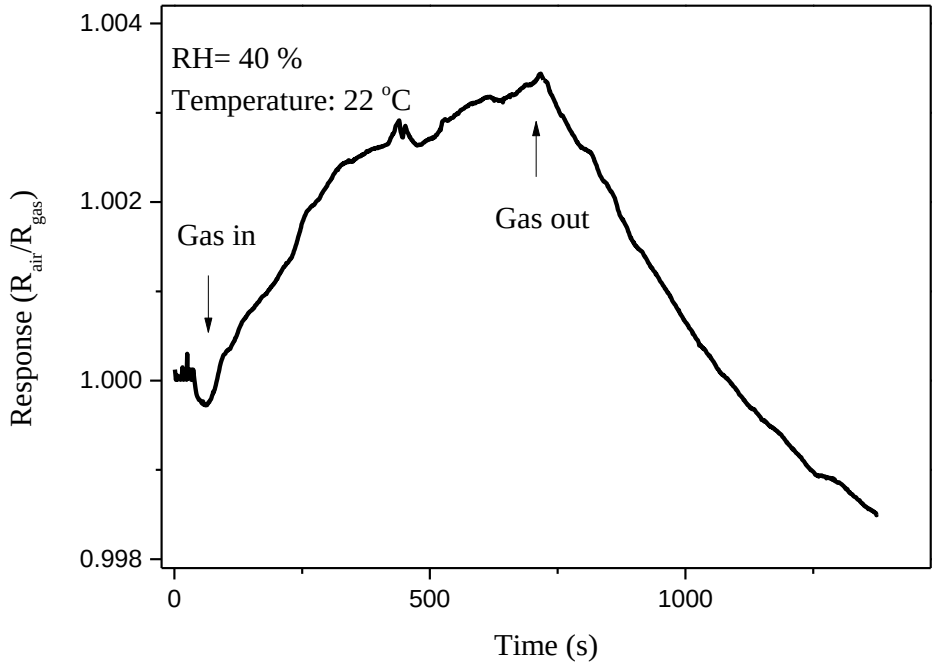
1.004
1.002
1.000
0.998
RH= 40 %
Temperature: 22 °C
Gas in
Gas out
0
500
1000
Response (R_{air}/R_{gas})
Time (s)

Fig.8

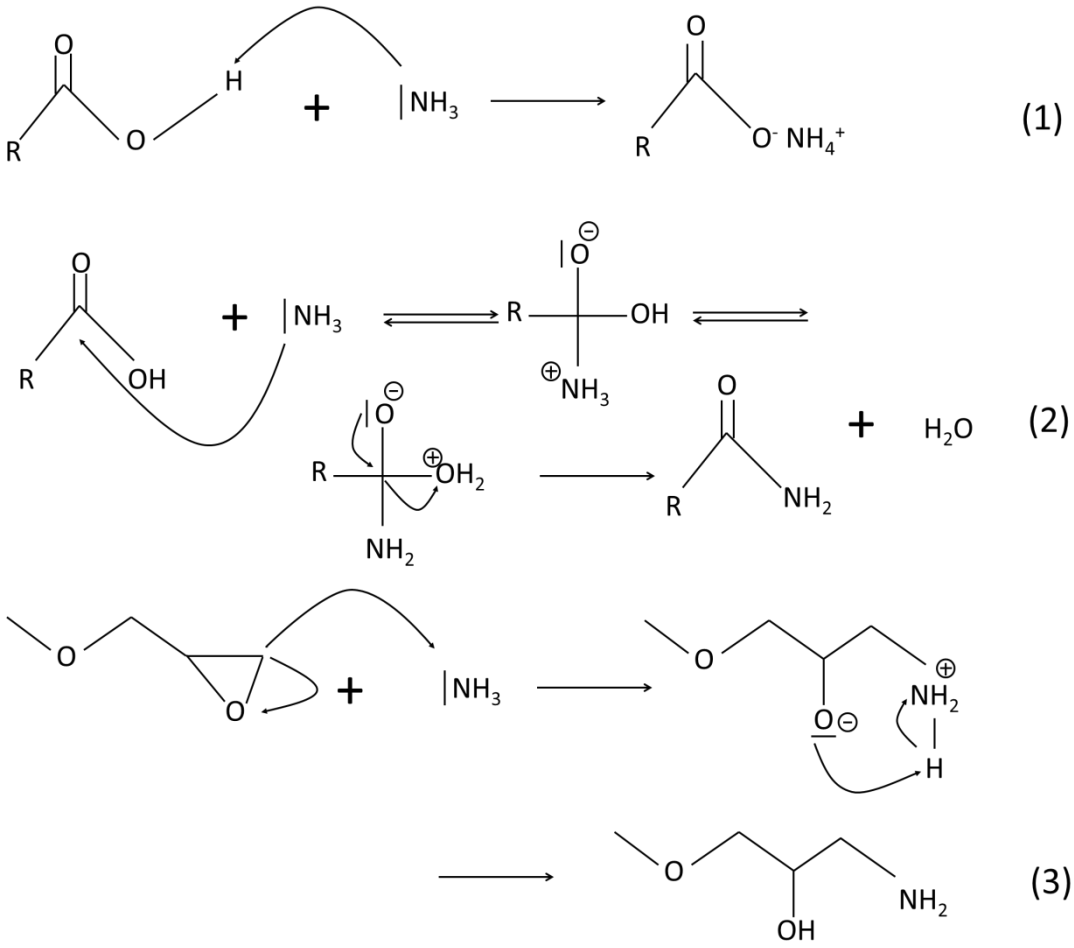
O
H
R
O
NH3
O
R
O- NH4+
(1)
O
R
OH
NH3
O
R
OH
NH3
O
R
OH2
NH2
O
R
NH2
H2O
(2)
O
O
NH3
O
O
NH2
H
O
OH
NH2
(3)

Fig.9(a)

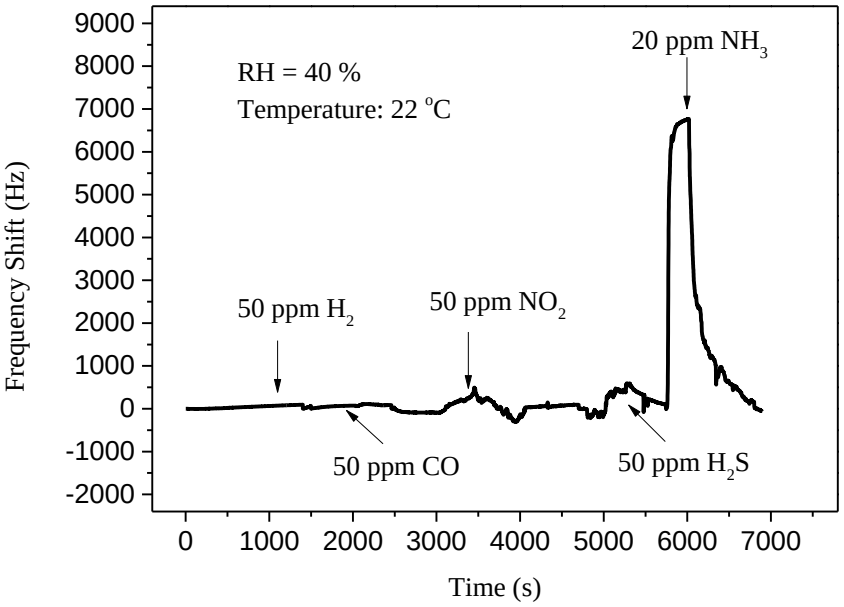
RH = 40 %
Temperature: 22 °C
20 ppm NH3
50 ppm H2
50 ppm NO2
50 ppm CO
50 ppm H2S
Frequency Shift (Hz)
Time (s)

Fig.9(b)

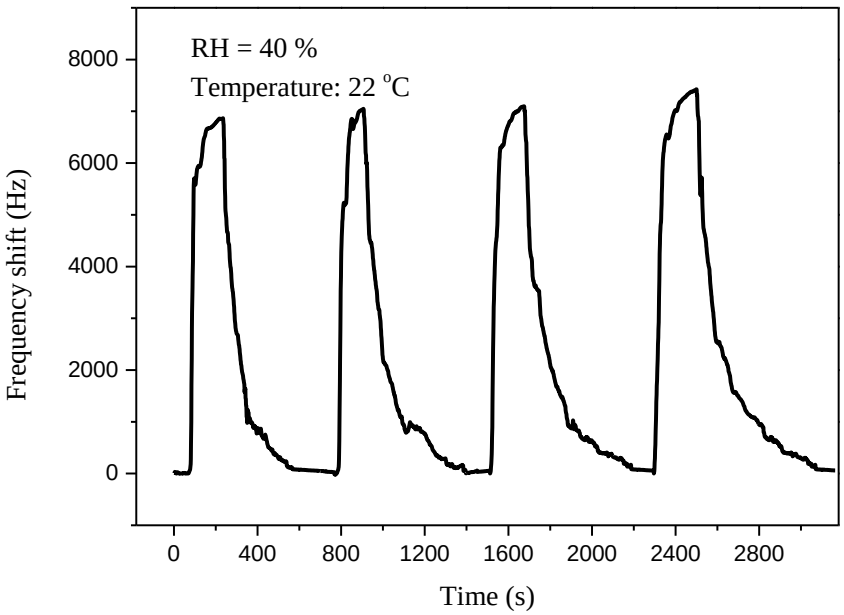
RH = 40 %
Temperature: 22 °C
Frequency shift (Hz)
Time (s)